





BRIEF REPORT



Analysis of *Drosophila* Atg8 proteins reveals multiple lipidation-independent roles

András Jipa ^{a,b}, Viktor Vedelek ^c, Zsolt Merényi^d, Adél Ürmösi^{a,b}, Szabolcs Takáts^e, Attila L. Kovács^e, Gábor V. Horváth^a, Rita Sinka ^c, and Gábor Juhász ^{a,e}

^aInstitute of Genetics, Biological Research Centre, Szeged, Hungary; ^bDoctoral School of Biology, University of Szeged, Szeged, Hungary; ^cDepartment of Genetics, University of Szeged, Szeged, Hungary; ^dInstitute of Biochemistry, Biological Research Centre, Szeged, Hungary; ^eDepartment of Anatomy, Cell and Developmental Biology, Eötvös Loránd University, Budapest, Hungary

ABSTRACT

Yeast Atg8 and its homologs are involved in autophagosome biogenesis in all eukaryotes. These are the most widely used markers for autophagy thanks to the association of their lipidated forms with autophagic membranes. The Atg8 protein family expanded in animals and plants, with most *Drosophila* species having two Atg8 homologs. In this Brief Report, we use clear-cut genetic analysis in *Drosophila melanogaster* to show that lipidated Atg8a is required for autophagy, while its non-lipidated form is essential for developmentally programmed larval midgut elimination and viability. In contrast, expression of Atg8b is restricted to the male germline and its loss causes male sterility without affecting autophagy. We find that high expression of non-lipidated Atg8b in the male germline is required for fertility. Consistent with these non-canonical functions of Atg8 proteins, loss of *Atg* genes required for Atg8 lipidation lead to autophagy defects but do not cause lethality or male sterility.

ARTICLE HISTORY

Received 11 May 2020
Revised 20 November 2020
Accepted 23 November 2020

KEYWORDS

Atg8a; Atg8b; autophagy;
Drosophila; sperm; testis



Introduction

Macroautophagy/autophagy is an evolutionarily conserved intracellular degradation process functioning in all eukaryotic organisms. During the main pathway, a membrane cistern (known as phagophore) is generated in the cytoplasm, and it grows around part of the cytoplasm, enclosing cargo into a double-membrane vesicle called autophagosome. Autophagosomes fuse with late endosomes and lysosomes to give rise to autolysosomes, in which the content and the inner membrane of autophagosomes are decomposed by hydrolytic enzymes [1]. This catabolic pathway plays a very important role in eukaryotic cells: the sustained turnover of macromolecules and organelles has an anti-aging effect, and it is essential for the adaptation to nutrient-poor conditions such as starvation. Besides these functions, autophagy has many other physiological and pathological functions [1].

Autophagy is mainly regulated by Tor (target of rapamycin) kinase and multiple Atg protein complexes [2]. In yeast, the Atg1 kinase complex (containing Atg1, Atg17, Atg13, and additional proteins that have no clear metazoan homologs) initiates autophagy in part via phosphorylation of the Vps34 lipid kinase complex (Vps34, Vps15, Vps30/Atg6 and Atg14, with the last subunit being responsible for the autophagy specificity of the complex), which phosphorylates the membrane lipid phosphatidylinositol to create PtdIns3P. This phospholipid serves as a signal that recruits PtdIns3P effectors


such as Atg18-family proteins. PtdIns3P-bound Atg18 is thought to bring along Atg2 to channel membrane lipids from other organelles such as the ER to the growing phagophore. The Atg18-Atg2 complex may also regulate the trafficking of vesicles positive for the transmembrane protein Atg9, which are also important for phagophore biogenesis. Lastly, Atg8 (the yeast homolog of mammalian MAP1LC3- and GABARAP-family proteins) is recruited to forming phagophores that is why this protein became the most widely used marker for autophagy: its redistribution from diffuse cytosolic to a punctate pattern indicates ongoing autophagy [2].

Atg8 belongs to the family of ubiquitin-like proteins, and its processing utilizes specific E1, E2 and E3-like activation steps similar to the process of ubiquitination [2]. Atg8 is first cleaved by the cysteine protease Atg4 to expose a glycine at its C-terminus. This cleavage is followed by a series of conjugation steps by the action of E1-like Atg7 and E2-like Atg3 enzymes, and the E3-like protein complex consisting of multimers of Atg16 and Atg12-Atg5 conjugates (with Atg12 also being a ubiquitin-like protein that is activated by Atg7 and the E2-like Atg10). Unlike ubiquitination, the target of Atg8 is the membrane lipid phosphatidylethanolamine rather than other proteins, which happens at autophagic membranes thanks to the localized action of the E3 complex. The covalent attachment of lipidated Atg8 (commonly referred to as Atg8-II) to autophagosomes promotes the elongation of the phagophore,

CONTACT Gábor Juhász  szmrt@elte.hu  Institute of Genetics, Biological Research Centre, Szeged, Hungary

Abbreviations:

Atg: autophagy-related; dj: don juan; GABARAP: Gamma-aminobutyric acid type A receptor-associated protein; MAP1LC3: microtubule associated protein 1 light chain 3; PtdIns3P: phosphatidylinositol-3-phosphate; ref(2)P/p62: refractory to sigma P; UAS: upstream activating sequence; Vps: vacuolar protein sorting.

 Supplemental data for this article can be accessed [here](#).

likely contributes to autophagosome closure, and Atg8 also acts as an anchor for selective autophagy receptors, motor protein adaptors and fusion factors that mediate autophagosome-lysosome fusion. Thus, Atg8 has crucial roles in general and selective autophagy, autophagosome trafficking and fusion with lysosomes [2].

Atg8 family proteins include MAP1LC3A, MAP1LC3B, MAP1LC3B2, MAP1LC3C, GABARAP, GABARAPL1, GABARAPL2 in mammals [2]. *Drosophila melanogaster* has two genes encoding Atg8 homologs: *Atg8a* and *Atg8b* [3]. Even though *Atg8a* is the most widely used experimental tool in this organism as well, fruit fly *Atg8* genes remained relatively uncharacterized. The gene of *Atg8a* has multiple transposon insertion alleles and derivatives, yet the proper characterization of their severity (hypomorphic vs. null alleles) is lacking. *Drosophila Atg8a* has been shown to function in the process of larval midgut shrinkage (a model of developmentally programmed cell death), unlike other members of the Atg8 conjugation system [4,5]. However, it is not clear whether *Atg8a* can be processed by an alternative conjugation system or it promotes this process in a non-lipidated form. *Atg8b* could be speculated to also act as a core gene in the process of autophagy, but high-throughput gene expression data reveal that *Atg8b* shows very strong expression in the testis and is barely detected in other tissues [6,7]. Yet, its role has remained a mystery.

In this study, we have generated and characterized null mutants for *Atg8a* and *Atg8b* genes and a conjugation-defective *Atg8a* missense mutant in *Drosophila*. Characterization of these new loss-of-function alleles allowed us to clarify the role of the two Atg8 homologs. We show that only *Atg8a* is involved in autophagy in various tissues including fat and testis, and its complete loss leads to a developmental delay, impairs developmental midgut elimination, and causes lethality at the late pupal stages. Interestingly, the conjugation-defective mutant that lacks the C-terminal glycine shows impaired autophagy but remains viable with proper development and midgut shrinkage, indicating lipidation-independent functions of *Atg8a*. We find that *Atg8b* expression is only seen in the male germline and it is required for male fertility, unlike other *Atg* gene products required for Atg8 conjugation and/or autophagy.

Results and discussion

At first, the evolution of Atg8 genes was reconstructed and visualized in a species tree, showing the number and type of Atg8 proteins in selected insect and closely related arthropod species (Figure 1A). This analysis revealed the presence of at least one Atg8 homolog (blue circle sections) in each species, as expected. An Atg8 paralog appeared early on (green circle sections) that has been lost in many species later on, including those that belong to the family of *Drosophilidae*. Interestingly, all *Drosophila* species have another Atg8 paralog (orange circle sections). In *Drosophila melanogaster*, these proteins are called *Atg8a* and *Atg8b*, respectively. Of note, it is the homologs of *Atg8a* that are found in all species that we analyzed, and the *Drosophilidae*-specific *Atg8b* gene probably arose in a retrotransposition event because it lacks introns [8].

The amino acid sequences of insect *Atg8a* and *Drosophilidae*-specific *Atg8b* proteins are very similar and are closer to the human GABARAP subfamily than to MAP1LC3 proteins (Fig. S1). In order to gain insight into the functions of *Atg8a* and *Atg8b*, we decided to generate genetic null alleles for both in *Drosophila melanogaster*. Previous functional studies of *Atg8a* by others and us relied on two viable alleles (Figure 1B): a P-element insertion into the protein-coding sequence in the first exon of the main *Atg8a* isoform (*Atg8a*^{KG07569}), and a molecularly defined deletion extending from this insertion site into the promoter region (*Atg8a*⁴⁴), which was generated by imprecise excision of this P element [9]. Importantly, high-throughput expression analyses identified the presence of two alternative *Atg8a* promoters, which can produce another two *Atg8a* isoforms that differ in their N-termini from the main isoform [10]. Thus, these two previously described *Atg8a* mutations are likely not genetic null alleles.

We took advantage of a *Minos* transposable element insertion (*Atg8a*^{MII3726}) in the first intron of *Atg8a* that is shared by all three alternatively spliced isoforms by inserting a new protein-coding exon called *Trojan-Gal4* into the *Minos* element that traps all isoforms [11]. This new insertion generated fusions between the very N-terminal parts of all *Atg8a* protein isoforms and a self-cleaving T2A polypeptide coupled to a yeast Gal4 transcription factor (a widely used genetic tool for driving the expression of genes containing a UAS promoter in *Drosophila*). The new allele (*Atg8a*^{Tro-Gal4}) thus prevented the expression of all *Atg8a* protein isoforms and was likely a genetic null (Figure 1B). This was supported by the late pupal lethality of *Atg8a*^{Tro-Gal4} mutant animals, and also by the accumulation of ref(2)P/p62 (refractory to sigma P; a receptor and selective autophagic cargo in *Drosophila*) [12] in western blots (Figure 1C and S2A). Of note, low ref(2)P levels were restored by introducing a *3xmCherry-Atg8a* transgene driven by its genomic promoter [13] in both *Atg8a*^{KG07569} and *Atg8a*^{Tro-Gal4} homozygous mutant larvae (Figure 1C and S2A).

The glycine residue located near the C-terminal end of Atg8 homologs is required for their lipidation [2]. This motivated us to generate a non-lipidatable mutant form that could be used for further functional analyses. We used the CRISPR-Cas9 system to introduce a point mutation into the endogenous *Atg8a* locus, which mutated the 116th glycine into a stop codon (Figure 1D). Animals carrying this *Atg8a*^{G116*} mutation indeed showed no sign of *Atg8a* lipidation (Figure 1E, Figure 1F and S2B) but were viable and fertile with no overall morphological alterations.

Since no mutants have been previously described for *Atg8b*, we again used CRISPR/Cas9 gene targeting to delete the whole protein-coding sequence of this gene (Figure 1G, Figure 1H). Unlike the *Atg8a*^{Tro-Gal4} mutation that appeared to eliminate the expression of *Atg8a* based on using a commercial anti-pan-GABARAP antibody (previously verified for recognizing *Drosophila Atg8* [14,15]) in western blots of larval lysates, the *Atg8b*¹⁶ gene deletion had no obvious effect on *Atg8a* protein levels in such samples (Figure 1E and S2B). This was in line with high-throughput expression analyses indicating that *Atg8b* is a testis-specific protein [6,7]. We

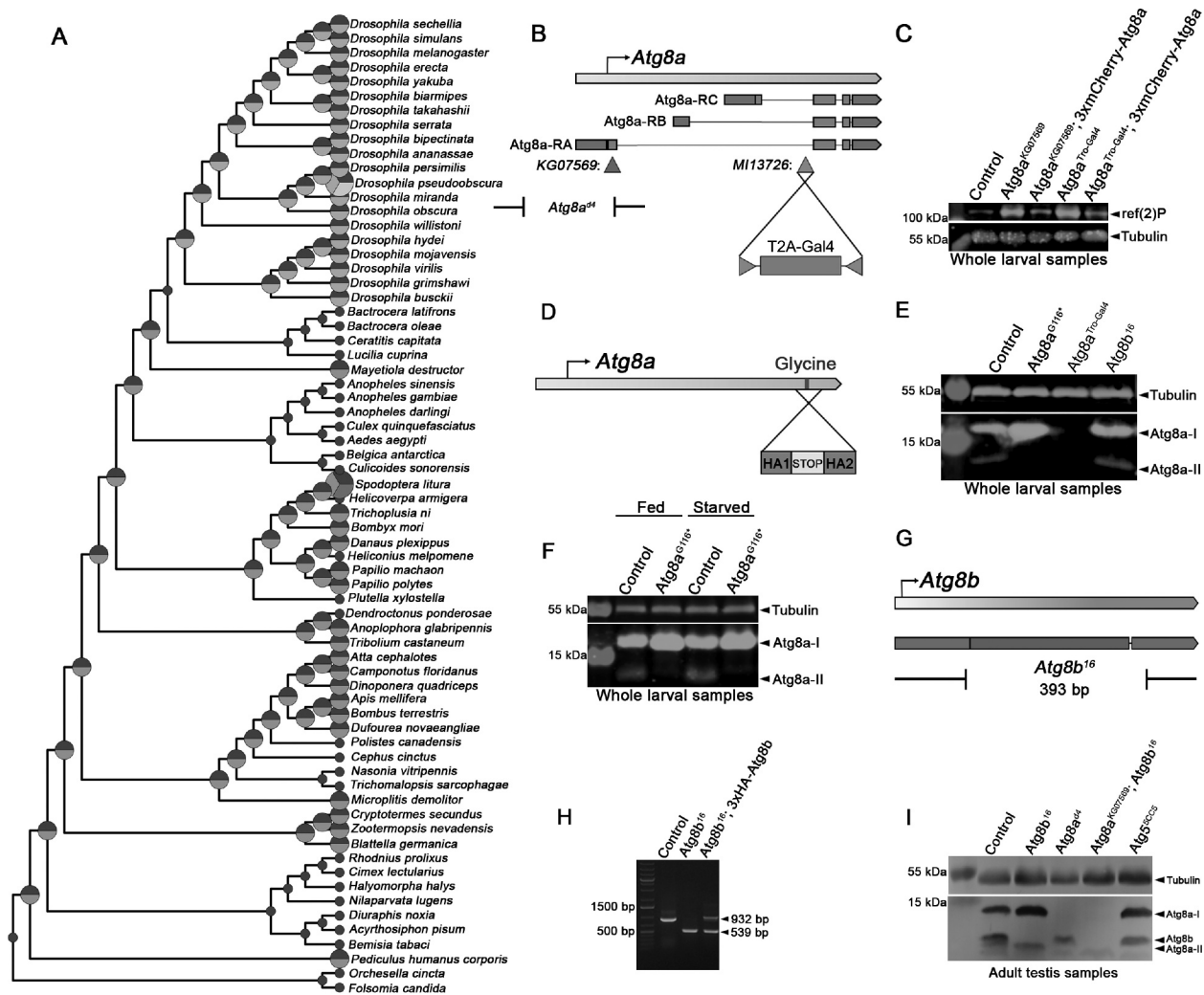


Figure 1. Generation of new *Atg8a* and *Atg8b* alleles. Reconstructed copy number evolution of *Atg8* family proteins in a species tree containing insects and closely related arthropods (A). Insects initially had two *Atg8* family proteins (blue and green circles/segments, respectively), but the second *Atg8* was lost in most species belonging to the order Diptera. *Drosophilidae* secondarily duplicated their *Atg8a* gene to give rise to a new paralog: *Atg8b* (whose protein product is indicated as an orange circle segment). (B) The *Atg8a* null allele was generated by inserting a *Trojan (T2A)-Gal4* cassette into the MI13726 transposon insertion situated in the first (biggest) intron of *Atg8a* (note that previous *Atg8a* alleles are also indicated in the gene map). The resulting *Atg8a^{Tro-Gal4}* gene trap likely disrupted all *Atg8a* gene products and caused accumulation of the autophagic cargo ref(2)P in western blots (C), which was comparable to the widely used P-element insertion allele (KG07569) located in the protein-coding first exon of the RA (main) transcript of *Atg8a*. Note that the normal, low ref(2)P level seen in controls was restored in *Atg8a* mutants by the expression of 3xmCherry-*Atg8a*. (D) The lipidation-deficient allele *Atg8a^{G116*}* was generated using an ssDNA-template for CRISPR/Cas9-mediated homologous recombination (D, HA1&2: homology arms). (E) No protein expression was seen in a western blot on *Atg8a^{Tro-Gal4}* mutant lysate, while *Atg8a* lipidation was blocked (there was no *Atg8a*-II) in starved *Atg8a^{G116*}* larvae unlike in starved control or *Atg8b* mutants. (F) Lipidated *Atg8a*-II was absent from homozygous *Atg8a^{G116*}* mutant larvae both in fed and starved conditions. (G) The *Atg8b¹⁶* null allele was generated using a double gRNA strategy to remove the entire *Atg8b* coding region by CRISPR/Cas9. (H) PCR analysis of genomic DNA samples confirmed the extent of deletion in *Atg8b* null mutants, and both the deletion and the wild type PCR fragment was seen in mutant animals containing a genomic promoter-driven 3xHA-*Atg8b* rescue transgene. (I) Expression of unmodified *Atg8a*-I, lipidated *Atg8a*-II and *Atg8b* in the testes of the indicated *Atg8a*, *Atg8b* and *Atg5* mutants. The faster migration of *Atg8b* compared to *Atg8a*-I was likely because of it being shorter by one amino acid and also because of its different amino acid sequence. Tubulin served as loading control on all western blots.

thus also analyzed adult testis samples by western blotting, which indeed detected *Atg8b* expression: a clear band corresponding to this protein was present in controls as well as viable *Atg8a^{d4}* and *Atg5^{5CC5}* mutant animals, with these *Atg8a* and *Atg5* mutants showing no expression or lack of lipidation of *Atg8a*, respectively (Figure 1I).

Next, we analyzed autophagic activity in the new *Atg8a* and *Atg8b* alleles using confocal microscopy. Immunofluorescent analyses using anti-GABARAP/*Atg8* detected no signal in *Atg8a^{Tro-Gal4}* mutant cell clones (marked by the lack of GFP) in mosaic fat tissue of starved larvae (Figure 2A), while a faint cloud-like signal was seen in *Atg8a^{G116*}* mutant cells (Figure

2B), likely representing nonlipidated *Atg8a*-I. LysoTracker Red is commonly used to stain acidic autolysosomes in *Drosophila* fat cells [3,16]. Both *Atg8a^{Tro-Gal4}* and *Atg8a^{G116*}* cell clones showed impaired starvation-induced punctate LysoTracker staining compared to neighboring control cells (Figure 2C, Figure 2D, S2C and S2D). Lastly, aggregates of the selective autophagy cargo GFP-ref(2)P accumulated in both *Atg8a^{Tro-Gal4}* and *Atg8a^{G116*}* mutant cell clones (marked by lack of RFP, Figure 2E, Figure 2F, S2E and S2F). These data altogether indicated that autophagy was blocked in cells homozygous for either of these *Atg8a* alleles, as expected. In contrast, punctate LysoTracker staining was indistinguishable in homozygous mutant *Atg8b¹⁶*

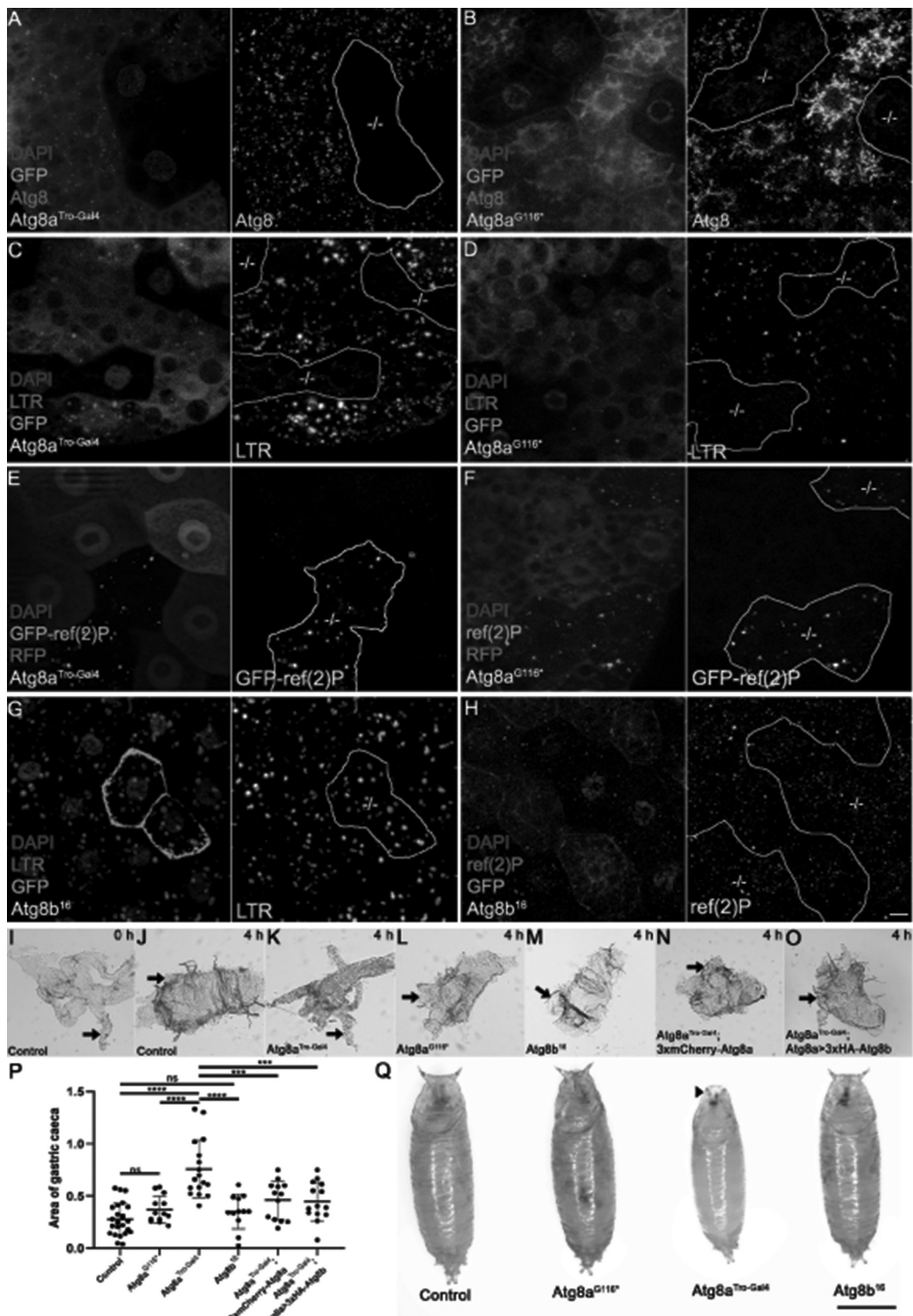


Figure 2. Atg8a: crucial for autophagy and development, unlike Atg8b. A commercial anti-GABARAP antibody that recognizes both Atg8 proteins in *Drosophila* was used for immunostainings of mosaic fat tissue in starved larvae with *Atg8a^{Tro-Gal4}* and *Atg8a^{G116*}* mutant cells marked by lack of GFP expression (A–D). No protein expression was seen in *Atg8a^{Tro-Gal4}* mutant cells (A) while a faint cloud-like signal is detected in the case of *Atg8a^{G116*}* cells. (B) Both *Atg8a^{Tro-Gal4}* and *Atg8a^{G116*}* mutant fat cells showed a strong decrease of starvation-induced punctate LysoTracker Red (LTR)-positive autolysosomal structures (C, D). Aggregates of GFP-ref(2)P (driven by the constitutive tubulin promoter) accumulated in both *Atg8a^{Tro-Gal4}* and *Atg8a^{G116*}* mutant larval fat cells that were marked by lack of RFP expression, compared to neighboring RFP-positive control cells (E, F). GFP-marked larval fat cells lacking Atg8b showed no difference in starvation-induced punctate LysoTracker Red (G) and endogenous ref(2)P staining (H) when compared to neighboring GFP-negative control cells. Note that -/- in grayscale panels of A–H indicate mutant cells. Panels I–O show the size of gastric caeca (arrows) in prepupae. Compared to the white prepupal stage (0 h, I), gastric caeca in the case of control (J), *Atg8a^{G116*}* (L) and *Atg8b¹⁶* (M) mainly regressed by 4 h later, while in *Atg8a^{Tro-Gal4}* mutants (L), the caeca remained almost intact. Interestingly, expression of either 3xCherry-Atg8a or 3xHA-Atg8b driven by the endogenous *Atg8a* promoter restored caeca regression in *Atg8a^{Tro-Gal4}* mutants (N, O). Panel P shows statistical analysis of data. $n = 12–24$ per genotype, **** $p < 0.0001$, ns: not significant based on one-way ANOVA. (Q) Pupal size of *Atg8a^{G116*}* and *Atg8b¹⁶* mutants was similar to control animals, however, *Atg8a^{Tro-Gal4}* mutants had reduced size and undeveloped anterior spiracles (arrowhead). Scale bars: 10 μm for A–H, 100 μm for I–O, and 1 mm for Q.

cell clones (marked by GFP) from neighboring control fat cells of starved larvae (Figure 2G and S2G), and there was no difference in the levels of endogenous ref(2)P between *Atg8b* mutant cells (marked by lack of GFP expression) and controls (Figure 2H and S2H). Thus, *Atg8b* was dispensable for autophagy in fat cells, in line with its testis-specific expression.

Elimination of the larval midgut epithelium during metamorphosis is considered to involve a form of developmentally programmed autophagic cell death/cell shrinkage. Surprisingly, proteins required for Atg8 lipidation turned out to be dispensable for this process, even though it requires most other *Atg* genes including *Atg8a* itself [4,5]. These previous studies left the question open whether this phenomenon is due to an alternative pathway of *Atg8a* lipidation or represents a lipidation-independent role of *Atg8a* in larval midgut elimination. To answer this question, we analyzed gastric ceca regression that largely takes place in the first 4 h of metamorphosis, as this process is commonly used to monitor larval midgut elimination [5]. The 4 gastric ceca are out-growths of the anterior larval midgut that were clearly visible at the time of puparium formation (indicated as 0 h) but largely disappeared by 4 h later (Figure 2I and Figure 2J). This process was strongly impaired in animals mutant for *Atg8a*^{Tro-Gal4} (Figure 2K and Figure 2P), in line with previous studies of *Atg8a* requirement [4,5]. However, gastric ceca regression happened normally in animals unable to lipidate *Atg8a* (Figure 2L and Figure 2P), pointing to a lipidation-independent role of *Atg8a* in this process. Lastly, the lack of *Atg8b* had no effect on developmental gastric ceca elimination either (Figure 2M and Figure 2P), in line with the testis-specific expression of this gene. Interestingly, impaired gastric ceca retraction of the *Atg8a*^{Tro-Gal4} mutant was rescued by endogenous *Atg8a* promoter-driven expression of either *Atg8a* or *Atg8b* (Figure 2N-P), indicating that both *Atg8* homologs had the potential to promote gastric ceca regression if present in this tissue. Similar phenotypes were also obvious in pupae (Figure 2Q): animals mutant for either *Atg8a*^{G116*} or *Atg8b*¹⁶ were viable and morphologically indistinguishable from controls, whereas *Atg8a*^{Tro-Gal4} null mutants were much smaller with defects in the eversion of anterior spiracles (respiratory openings) and all died before eclosion.

To gain further insight into the function of *Atg8a* and *Atg8b*, we looked at their expression patterns. Our previously described 3xmCherry-*Atg8a* reporter that is driven by the endogenous *Atg8a* promoter and contains all *Atg8a* exons and introns [13] showed universal expression in all tissues (Figure 3A), in line with its important role in autophagy in all cells. We also generated a 3xeGFP-*Atg8b* reporter driven by the endogenous *Atg8b* promoter. The expression of this transgene was only detected in the developing testis in larvae (Figure 3A). We thus turned to analyze the expression of these proteins in the adult testis (please see Figure 3B for a schematic tissue composition of this organ). Transgenic 3xmCherry-*Atg8a* expression was detected in both the germline and somatic cells of the testis (Figure 3C,D). In contrast, transgenic 3xGFP-*Atg8b* was highly expressed in the germline and was absent from somatic cells (Figure 3C and Figure 3E). During spermiogenesis, both *Atg8a* and *Atg8b* displayed punctate distribution with a diffuse background in early

cysts (encircled in Figure 3C-E). Interestingly, while *Atg8a* expression strongly decreased in post-meiotic stages (Figure 3C,D), the high-level expression of *Atg8b* was maintained in these elongated cysts, and *Atg8b* was clearly associated with the tail region of spermatids (Figure 3C and Figure 3E).

These observations prompted us to carry out fertility tests with males mutant for different *Atg* genes. Crossing these *Atg* mutants to control females revealed that only *Atg8b* mutant males were sterile, unlike *Atg5*, *Atg7*, *Atg16* (note that the corresponding proteins are necessary for *Atg8* lipidation), *Atg101* (encoding an *Atg1* kinase subunit) and *Atg9* (encoding a transmembrane protein) null mutant males (Figure 3F). While a subset of *Atg8a*^{G116*} mutant males were also sterile in our tests, this was likely due to defects in wing unfolding that were observed at a low penetrance, as most males homozygous for this mutation managed to produce offspring (Figure 3F). Although autophagy is important to prevent a decline in fertility over time owing to the need for long-term maintenance of stem cells [17], all of the viable *Atg* mutants that we tested can be maintained as homozygous stocks with the exception of male-sterile *Atg8b* nulls (this study) and female sterile *Atg9* nulls [18].

To understand the reason for the sterility of *Atg8b* mutant males, we conducted microscopic analysis on dissected testis samples, looking for aberrations in characteristic developmental stages [19]. We did not observe abnormalities in the early developmental stages, as the 16-cell cysts containing primary spermatocytes were formed and meiosis seemed to proceed normally in the mutant. After meiosis the spermatids start to elongate, giving rise to elongated cysts in both control and mutant males, therefore this process was not affected in *Atg8b* null males. After elongation, the next developmental step is individualization. During this, the individualization complex (which consists of actin-rich, cone-shaped cytoskeletal structures) forms at the apical end of the cyst and starts its migration to the basal end. The majority of cytosolic components are degraded and expelled to the waste bag, and at the end of the process, the individual sperm forms. For spermatid individualization, directed protein degradation by proteasomes and non-apoptotic caspase activity are essential. We visualized caspase activity with anti-active drice antibody and migrating actin cones with fluorophore-conjugated phalloidin (Fig. S3A). We found that the individualization process proceeded normally in *Atg8b* mutants, and the morphology of the individualization complex was similar to the controls, and the non-apoptotic caspase cascade was active in the forming waste bags. After individualization, the next step is the coiling and transfer of the mature sperm to the seminal vesicle. We studied this step by visualizing mature polyglycylated axonemal tubulins with the AXO49 antibody (Fig. S3B). This analysis indicated that mature sperm formed in the *Atg8b* mutant, but its proper transfer was defective. In line with this, the enlargement of the proximal part of the testis due to accumulation of sperm was obvious in *Atg8b* mutant males (Figure 3G,H). To test if the sperms reaching the seminal vesicle were transferred to the females or not, we marked them with dj-GFP that properly labels both control and *Atg8b* mutant sperm cells (Fig. S3C). After mating these males to control females, we dissected the female sperm

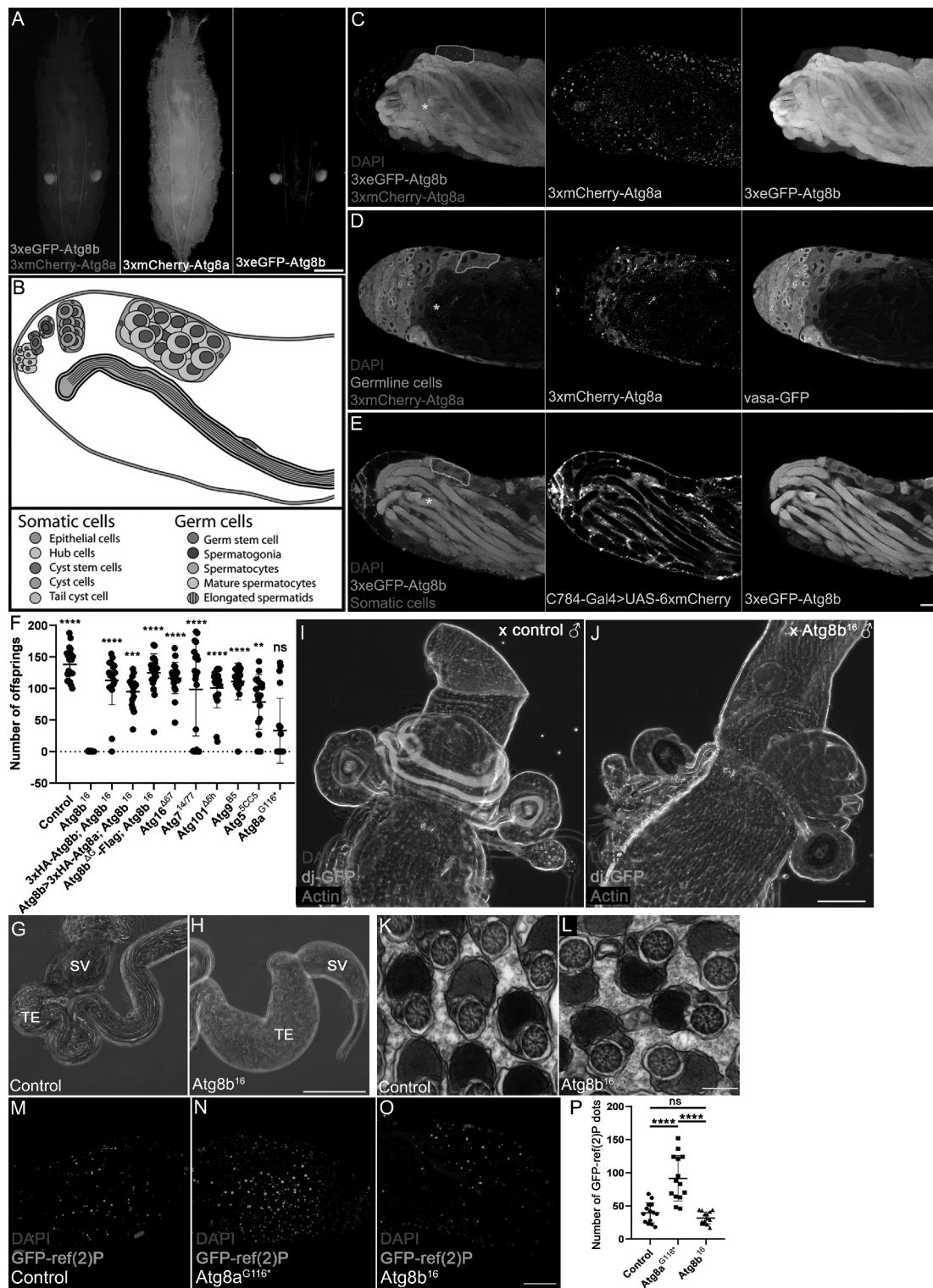


Figure 3. Atg8b: required for male fertility independent of lipidation and autophagy. (A) The genomic *Atg8a* promoter-driven *3xmCherry-Atg8a* transgene (red) showed a general expression pattern, while the genomic *Atg8b* promoter-driven *3xeGFP-Atg8b* transgene (green) was expressed only in the paired developing testes. Note the weak autofluorescence of the dorsal tracheal trunks and gut contents. (B) Schematic illustration of the tissue composition of the adult fruit fly testis. (C) Co-expression analysis of the *Atg8a* and *Atg8b* expressing transgenes in the adult testis revealed *Atg8b* expression (green) only in the male germline (starting approximately in the 4–16 cell cyst stage – note that one cyst is circled in each of panels C–E), while *Atg8a* (red) was seen in all cells, although its expression level was lower in elongated cysts (marked by *). (D) Co-expression analysis of *3xmCherry-Atg8a* and germline-specific *Vasa-GFP* showed that *Atg8a* had stronger expression in somatic cells (note its more punctate pattern in epithelial cells near the testis surface and in hub cells seen on the left side). (E) Somatic cyst cell-specific expression of mCherry using *C784-Gal4* showed mutually exclusive pattern with *3xeGFP-Atg8b*, indicating the male germline-specific expression of *Atg8b*. (F) Number of offsprings after crossing 1 male of the indicated genotypes with 2 wild type females. All *Atg* mutants showed higher male fertility than the *Atg8b¹⁶* allele, and this male-sterile phenotype was rescued by endogenous *Atg8b* promoter-driven *Atg8b* and *Atg8a* transgenes. Data was analyzed by Kruskal-Wallis test, $n = 20$ /genotype, ****: $p < 0.0001$, ***: $p < 0.001$, **: $p < 0.01$, *: $p < 0.05$, ns: not significant. (G, H) The base of dissected testis in 10-d-old male flies. The terminal epithelium (TE, containing coiled mature spermatids that attach here) and seminal vesicle (SV, storing mature sperm before release) in a control fly (G). The *Atg8b¹⁶* mutant testis featured a massively enlarged terminal epithelium (TE) due to the accumulation of immobile sperm cells (H). (I) The spermatheca and receptacle seminis of a wild

type female mated with a control dj-GFP transgenic male contained sperm (green). (J) In contrast, both sperm storing organs were empty when a wild-type female was mated with an *Atg8b*¹⁶ mutant male expressing dj-GFP. Transmission electron micrographs of cross-sectioned testes from control (K) and *Atg8b*¹⁶ mutant flies (L). In both control and mutant testis, well-organized spermatocyte cysts were seen with indistinguishable ultrastructure of spermatid tails. The number of GFP-ref(2)P dots in the apical part of control (M) and *Atg8b*¹⁶ mutant (O) testes were similar, while it significantly increased in *Atg8a*^{G116*} (N) testis, suggesting that *Atg8b* fulfills its function in male fertility in an autophagy-independent manner. Data was evaluated by one-way ANOVA (P), n = 14/genotype, ****: p < 0.0001, ns: not significant. Scale bar: 250 μ m for A, 200 μ m for C-E, 100 μ m for G, H, 100 μ m for I, J, 100 nm for K, L, and 50 μ m for M-O.

storage organs. These experiments revealed that *Atg8b* mutant sperm cells failed to reach the seminal receptacle and spermatheca of mated control females (Figure 3I,J). This result was probably due to the low motility of mutant sperm cells (Videos S1 and S2). Since transmission electron microscopy showed normal spermatid ultrastructure in the developing cysts in *Atg8b* mutants, as the axoneme and the two mitochondrial derivatives formed normally (Figure 3K,L), these suggested that *Atg8b* did not function as a structural protein in spermiogenesis. Taken together, we pinpointed the role of *Atg8b* at the late stages of post-meiotic spermatid development and motility.

Our analysis of multiple viable *Atg* mutants suggested that it was likely not autophagy that causes infertility in *Atg8b* mutant *Drosophila* males. We also tested the importance of potential *Atg8b* lipidation. Transgenic expression of full-length *Atg8b* driven by its endogenous promoter readily rescued the male sterility of *Atg8b* null mutants, similar to an *Atg8b* ^{Δ G-Flag} transgene lacking the glycine residue in the C-terminal part of the protein that would be critical for lipidation (Figure 3F). We also assessed autophagy in the testis by counting the number of GFP-ref(2)P dots in testis samples. Similar to our fat cell data, GFP-ref(2)P aggregates accumulated in *Atg8a* mutants compared to control and *Atg8b*^{G116*} mutant males (Figure 3M-P). These results, together with *Atg8b* always appearing as a single band in western blots (Figure 1I) and that proteins involved in *Atg8* lipidation and autophagy were dispensable for male fertility, strongly supported a lipidation- and autophagy-independent role for *Atg8b* in this process. Interestingly, while the amino acid sequence of *Atg8b* orthologs was almost identical among various *Drosophila* species, in *Drosophila obscura*, *persimilis*, *miranda*, *guanche*, and *pseudoobscura* (all belonging to the *obscura* group) a C-terminal truncation of a few amino acids led to complete loss of the glycine that would be essential for lipidation (Fig. S1), further supporting that *Atg8b* lipid conjugation was not critical for its testis function. One possibility is a potential microtubule-associated role (note that the abbreviation MAP1LC3 stands for microtubule associated protein 1 light chain 3 in human homologs) that is also in line with the localization of *Atg8b* in the tails of elongating spermatids. Interestingly, the *Atg8b* mutant phenotype manifested after individualization, where the sperm cells already had minimal cytosol, and the axoneme was surrounded by an ER-derived double membrane. Since all these specialized structures form normally in the absence of *Atg8b* based on ultrastructural analysis, the exact role of *Atg8b* in the testis remained unclear.

The last question we sought to answer was: what is so special about *Atg8b*? Is it required for male fertility because of its high expression in the male germline so that the lower expression of *Atg8a* cannot compensate for its loss, or did the function of this protein diverge from that of *Atg8a*? To this

end, we generated an *Atg8a* transgene driven by the testis-specific promoter of *Atg8b*. Expression of this construct perfectly restored male fertility in *Atg8b* mutants (Figure 3F), suggesting that a high level of either non-lipidated *Atg8* protein is sufficient for male fertility in *Drosophila*. The testis-specific function of *Atg8b* is consistent with the common generation of new autosomal retrogenes with testis-specific expression (including *Atg8b*) from X-linked genes (including *Atg8a*), a process that is likely driven by X chromosome inactivation during late spermatogenesis in both *Drosophila* and mammals [8]. Our data pointed to a potential general importance of *Atg8* family proteins in male fertility independent of lipidation and autophagy, which would be exciting to study in mammals, but it is challenging due to the presence of 7 paralogs.

Autophagy has been suggested to contribute to male fertility in mammals via, for example, ensuring proper lipid homeostasis for testosterone production in Leydig cells [20], but this is clearly not the case in *Drosophila*. Lipidation-independent functions of *Atg8* family proteins have also been reported in mammals. Unlipidated MAP1LC3 proteins are associated with intracellular *Chlamydia* and it is important for the propagation of bacteria, while inhibition of autophagy enhanced chlamydial growth [21]. Unlipidated MAP1LC3 proteins coat EDEMosomes: ER-derived vesicles transporting ER chaperones including EDEM1 to endosomes for breakdown [22]. Of note, coronaviruses are known to hijack this pathway to generate double-membrane vesicles (DMVs) that aid virus replication [23]. Thus, understanding lipidation-independent functions of *Atg8* family proteins has clear medical relevance, especially considering the coronavirus pandemic started at the end of 2019.

Taken together, we showed that *Atg8a* was important for developmentally programmed removal of larval gastric ceca, for proper pupal development and for the eclosion of adult flies. These were all independent of its lipidation based on analysis of the unlipidatable mutant, likely reflecting an autophagy-independent role of *Atg8a* in these processes. We also showed that high expression of *Atg8b* was required for male fertility independent of its lipidation and autophagy. The new mutant and transgenic animals generated in this study will be useful to further study these exciting phenomena.

Materials and methods

Fly work

Flies were kept on standard yeast (Vizyon, 5,998200460746), corn (Paco, 5,997975390784) and agar (Molar, 00673-702-190)-based medium at 25°C unless otherwise noted. For fertility tests, we used freshly eclosed male flies crossed individually with two w¹¹¹⁸ virgin females, and they were cultured on

the same medium. After 5 d, we removed the females, and 5 d after eclosion, we counted the progeny in individual vials. For starvation experiments, early L3 stage larvae were floated on top of a 20% sucrose (VWR, 57–50-1) solution at 25°C for 3 h. For somatic mutant clones generation in the fat body, 0–4 h old embryos were heat-shocked for 45 min in a 37°C temperature bath.

The following *Drosophila* lines were used: *Atg8a^{Tro-GAL4}*, *Atg8a^{G116*}*, *Atg8b¹⁶*, *Atg8b>3xeGFP-Atg8b*, *Atg8b>3xHA-Atg8b*, *Atg8a>3xHA-Atg8b*, *Atg8b>3xHA-Atg8b^{ΔG}-Flag* (all described in this study), *Atg7^{14/77}* [24], *Atg101^{Δ6h}* [25], *Atg9^{B5}* [18], *Atg5^{5CC5}* [26], *Atg16^{Δ67}* [27], *tubulin>GFP-ref(2)P* [13], *3xmCherry-Atg8a* [13], *Atg8a^{MI13726}*, *lox2-attB2-SA-T2A-Gal4-Hsp70*; *Dr/TM3 Sb Cre vas-int.Dm*, *UAS-2xeGFP*, *C784-Gal4*, *Act5C-Cas9.P.RFP*, *DNAIig4¹⁶⁹ Act5C-Cas9* (all obtained from the Bloomington *Drosophila* Stock Center), *dj-GFP* [28], *vasa-GFP* [29].

Generation of *Atg8a* and *Atg8b* mutants

To generate the *Atg8a^{Tro-Gal4}* null allele, we used Plug-and-Play gene trapping methods [11]. First, using standard genetic crossings, we generated flies that simultaneously contain the *Atg8a^{MI13726}* *Minos* element, *pC-(lox2-attB2-SA-T2A-Gal4-Hsp70)3* donor cassette, and *Cre vas-int.Dm* a *Cre* recombinase and a ϕ C31 integrase source. This line was crossed with *UAS-2xeGFP* and we screened for suitable candidates among the progeny based on GFP expression driven by the correctly inserted *Trojan-Gal4* exon.

To generate the *Atg8a^{G116*}* lipidation-defective mutant, we used a CRISPR/Cas9-mediated homologous recombination *in vivo* mutagenesis method [30]. The gRNA sequences were cloned into the Bbs1 (NEB, R0539S) site of the pCFD5 (Addgene, 73914, deposited by Simon Bullock) plasmid using the oligonucleotides: *Atg8a_1*: TGCACGATGAGAATGTTTACGGCA and *Atg8a_2*: AAAGTCCGTAACATTCTCATCG. This guide RNA carrier clone was co-injected into *Act5C-Cas9 lig4¹⁶⁹* fly eggs together with a ssDNA template containing two homologous arms and the desired change (glycine 116 to a stop codon):

TAGGAACATCACGAGGAGGACTATTCCTGTACATT-GCCTACTCCGATGAGAATGTTTACTAAATGGCCAAA-ATTAACAACTTTGCTCCGGTCGGGATGCATCGGAA-TGAAGCCCCCCCCCT. Candidate lines were screened by immunoblot for accumulation of the autophagy-specific cargo ref(2)P, followed by confirmation with sequencing.

To generate the *Atg8b¹⁶* null allele we first created a double gRNA bearing construct using two pairs of oligonucleotides: CTTCGTAGTTCATATCCATCTGGG, AAACCCAGATGGATATGAACTAC and CTTCGACTCGCGTAATCGTTTTGG, AAACCCAAAACGATTACGCGAGTC. These oligonucleotides were annealed and cloned into the pBFv-U6.2B (Addgene, 138401, deposited by Shu Kondo) vector as described [31]. We then generated an *Atg8b* gRNA transgenic fly line and crossed it with *act5C>Cas9* transgenic flies. We screened candidate mutant lines by PCR using *Atg8b* specific primers (*Atg8b_1*: GGGATTAGCGGATGCTATGCAC

Atg8b_2: CCCCTAGGGAAATTTGGCACTC) and identified the *Atg8b¹⁶* allele that carries a 393 bp deletion based on sequencing data.

To generate somatic mutant fat body clones, the *Atg8a* mutants were first recombined to an *FRT19A* containing chromosome, and then these lines were crossed with *hsFlp*, *FRT19A ubi-RFP* (or *ubi-GFP*) flies. To generate positively or negatively labeled somatic mutant fat body clones, the *Atg8b¹⁶* mutant was recombined to an *FRT82B* containing chromosome, and then these lines were crossed either with *hs-Flp*; *QUAS-mCD8-GFP* or *RFP*; *ET49-QF*, *FRT82B tub-QS/TM6* or with *hsFlp*; *r4> Gal4*, *FRT82B*, *UAS-GFP*.

Molecular cloning and generation of transgenic animals

For the generation of endogenous promoter-driven *3xeGFP-Atg8b* reporter transgene, we first amplified by PCR the *Atg8b* 5'-UTR promoter region using genomic fly DNA as a template and ATCAATTGCATGCCAGGCGGACACGATTAAGTGG and GACTGAATTCTGGGCGGACTGGAATACGGTT primers and then cloned it into pUAST-attB-3xGFP (Addgene, 85621) vector as an *SphI* (NEB, R3182)-*EcoRI* (NEB, R3101) fragment (pGen-3xGFP). Second, the coding and the 3'-UTR region of *Atg8b* was amplified using GATATAGCGGCCGCGGAGGTGGCATGGATATGAACTA-CCAGTACAAGAAGG and CTCGAGGTACCAGCCGATCAGTTTGCACGCTTC primers and cloned it into the above vector as a *NotI* (NEB, R3189)-*Acc65I* (NEB, R0599S) fragment.

To generate the C-terminal FLAG-containing *Atg8b* construct lacking the glycine at position 118 (*Atg8b^{ΔG}-Flag*), an intermediate construct was first created. The coding region of *Atg8b* gene without the glycine 118 coding triplet but containing a C-terminal FLAG coding sequence along with 18 nucleotides of the 3'-UTR was amplified with *Atg8bFWD*: AATAGAATTCATGGATATGAACTACCAGTACAAGAA-GGAC and *Atg8bFLAGUTRREV*: AATTCTCGAGTCAAGCCCGCTCTACTTGTTCATCGTC-GTCCTTGTAGTCCGCGTCCATAGACGTTCTCAT primers, and the PCR product was cloned into the *EcoRI* (NEB, R3101) – *XhoI* (NEB, R0146S) site of pBluescript SK (+) vector (Stratagene, 212205) (pBluescript-*Atg8b* [1-117]-FLAG). The 3'-UTR of *Atg8b* was amplified with *XhoUTRREV*: GGGCTTGACTCGAGTAATCGTT and *Acc65IUTRREV*: TAGAGGTACCAGCCGATCAGT primers and the *XhoI* (NEB, R0146S)-*Acc65I* (NEB, R0599S) digested PCR product was ligated with *XhoI* (NEB, R0146S)-*Acc65I* (NEB, R0599S) digested pBluescript-*Atg8b*(1-117)-FLAG. Then the *EcoRI*-*Acc65I* fragment containing the *Atg8b* (1-117)-FLAG-3'UTR was ligated with *EcoRI* (NEB, R3101)-*Acc65I* (NEB, R0599S) digested pGen-3xGFP plasmid, resulting in the pGen-*Atg8b*(1-117)-FLAG-UTR construct.

The *Atg8b* encoding construct with N-terminal 3xHA tag was generated as follows: 3xHA tag encoding sequence was amplified with HAFWD: TACCGAATTCATGTACCCATACGATGTTTCTCCT and HAREV: ATAACCTCGAGAGCGTAATCTGGAACGTCATA from the *UAS-3xHA-VAMP7* plasmid [32]. Following *EcoRI* (NEB, R3101)-*XhoI* (NEB, R0146S) double digestion, the

resulting fragment was ligated with similarly digested pBluescript SK (+) vector. The *Atg8b* coding region with the 3'-UTR was amplified with *Atg8bXhoFWD*: AAGGCTCGAGATGGATATGAACTACCAGTACAAGAAG and *Acc65IUTRREV* primers and after *XhoI* (NEB, R0146S)-*Acc65I* (NEB, R0599S) digestion the fragment was inserted between the *XhoI*-*Acc65I* sites of pBluescript SK (+)-3xHA. The *EcoRI*-*Acc65I* fragment of this plasmid (encoding 3xHA-*Atg8b* with the 3'-UTR region) was cloned into an empty pGen plasmid [33] giving rise to pGen-3xHA-*Atg8b*-UTR.

The 3xHA-tagged *Atg8a* construct driven by the *Atg8b* promoter and 3'-UTR was generated by amplification of *Atg8a* coding sequence with *Atg8aXhoFWD*: AAGGCTCGAGATGAAGTTCCAATACAAGGAGGAGC and *Atg8aBglIIREV*:

TTAAAGATCTAGTTAATTTTGGCCATGCCGTAA primers, *Atg8b* 3'-UTR with *Atg8bUTRBGLIIFWD*: AATTAGATCTCGCGGGCTTGACTCG and *Atg8bUTRAcc65IREV*: TAGAGGTACCAGCCGATCAGT primers and following *XhoI* (NEB, R0146S)-*BglII* (R0144S) and *BglII* (R0144S)-*Acc65I* (NEB, R0599S) double digestions, the purified fragments were ligated with *XhoI* (NEB, R0146S)-*Acc65I* (NEB, R0599S) digested pBluescript SK (+)-3xHA. After sequence verification, the *XhoI*-*Acc65I* fragment of this construct was cloned into the pGen plasmid resulting in pGen-*Atg8b* promoter-3xHA-*Atg8a*-*Atg8b* 3'-UTR construct.

pUAST-attB-*Atg8a*prom-3XHA-*Atg8b*-*Atg8a*UTR plasmid was constructed as follows: pBluescript SK (+)-3xHA-*Atg8b* plasmid was digested with *BglII* (R0144S)-*Acc65I* (NEB, R0599S) enzymes and ligated with *Atg8a* 3'UTR fragment amplified with *Atg8aUTRFWD*: TTTTGATCCTTTGCTCCGGTCCGGATGCA and *Atg8aUTRAccREV*: TAGAGGTACCAAACTGCGAGGCCA primers and digested with *BamHI* (NEB, R3136)-*Acc65I* (NEB, R0599S) enzymes. This resulted in pBSK 3xHA-*Atg8b*-*Atg8a*UTR intermediate construct. pGen-3xHA-*Atg8b*-UTR plasmid was digested with *SphI* (NEB, R0182S)-*EcoRI* (NEB, R3101) enzymes and ligated with *SphI* (NEB, R0182S)-*EcoRI* (R0101S) digested *Atg8a* promoter fragment, amplified with *Atg8aPROMFWD*: CTTGCATGCGAATGTGATTGATCA and *Atg8aPROMREV*: CCATGAATTTCGATTGCAATGAAGAGGTAATTG primers, resulting in pUAST-attB-*Atg8a*prom-*Atg8b*-UTR construct. pUAST-attB-*Atg8a*prom-3XHA-*Atg8b*-*Atg8a*UTR construct was generated with NEBuilder® HiFi DNA Assembly Master Mix (NEB, E2621 G) according to manufacturer's instructions using *EcoRI* (R0101S)-*Acc65I* (NEB, R0599S) digested pUAST-attB-*Atg8a*prom-*Atg8b*-UTR construct and 3xHA-*Atg8b*-*Atg8a*UTR PCR fragment amplified with *GAecoRIFWD*: AGCCAATTACCTCTTCATTGCAATCGAATTCATGTACCCATACGATGTTCTCG and *GAAcc65REV*: CCTTACAAAGATCCTCTAGAGGTACCAAACTGCGAGGCCAAC primers from pBSK-3xHA-*Atg8b*-*Atg8a*UTR plasmid as template.

All constructs have been fully sequenced and new transgenic lines were generated at the in-house *Drosophila* Injection Facility, BRC, Szeged.

Fluorescent imaging, immunostaining and microscopy

For LTR staining, fat bodies of early L3 larvae starved for 3 h were dissected and incubated in 35 μ L PBS (PanReac AppliChem, A9177,0100) containing 100 μ M LysoTracker Red (Invitrogen, L7528) and 0.2 μ g/ml DAPI (Invitrogen, D1306) for 5 min then samples were washed in PBS and mounted in 50% glycerol (Sigma, G5516-1 L) in PBS.

For immunostainings, early L3 larvae were processed as described [13,18]. The following primary antibodies were used: polyclonal rabbit anti-ref(2)P (1:1,000) [34], monoclonal chicken anti-GFP (1:1,000; Aveslab, GFP-1020), rabbit monoclonal anti-Gabarap+GabarapL1+ GabarapL2 (1:400; Abcam, ab109364). The following secondary antibodies were used: anti-rabbit Alexa Fluor 568 (1:800; Life Technologies, A11036), anti-chicken Alexa Fluor 488 (1:800; Thermo Fisher Scientific, SA5-10070).

We dissected spermatheca from fertilized females were dissected in PBS. The obtained tissues were fixed in 4% FA, then washed in PBST (PBS containing 0.1% Triton X-100 [Sigma-Aldrich, T8787]) for 3 \times 10 min. DAPI (Invitrogen, D1306) was used at 1 μ g/ml concentration, Texas Red-X Phalloidin (Thermo Fisher Scientific, T7471) was used at a dilution of 1:250 for 30 min. Samples were mounted in SlowFade Gold antifade reagent (Life Technologies, S36936).

Testis dissection and staining procedures were performed as described earlier [35]. Texas Red-X Phalloidin (Thermo Fisher Scientific, T7471) was used in a dilution of 1:250. Rabbit anti-cleaved-CASP3 (caspase 3; Cell Signaling Technology, clone 5A1E, 9664) was used in 1:200, mouse anti-pan polyglycylated tubulin antibody (Merck, clone AXO 49, MABS276) was used in 1:5,000 dilution. Alexa Fluor 488 conjugated anti-mouse and anti-rabbit antibodies (Invitrogen, Z25002, Z25302) were used as secondary antibodies (1:400). Samples were mounted in SlowFade Gold antifade reagent (Life Technologies, S36936). Images were taken by Olympus BX51 fluorescent microscope or by a Zeiss AxioImager M2 microscope equipped with an ApoTome 2 grid confocal module and an ORCA-Flash4.0 LT sCMOS camera (Hamamatsu). Spermatheca images were taken on an Olympus Fluoview Fv10i Confocal microscope. Images were processed in ZEN Lite 3.1, Photoshop CS3 (Adobe) and ImageJ (NIH).

Electron microscopy analyses of dissected testes were processed for ultrastructural analysis as before [35]. Images were taken using a JEOL JEM-1011 transmission electron microscope equipped with an Olympus Morada camera and iTEM software.

Immunoblotting

The protocols of the immunoblotting experiments were described previously [36]. In the case of fluorescence-based experiments, we used Immobilon-FL PVDF membrane (Merck, IPFL00010). Primary antibodies were polyclonal rabbit anti-ref(2)P (1:4,000) [34], rabbit monoclonal anti-Gabarap+GabarapL1+ GabarapL2 (1:2,000; Abcam, ab109364), and mouse anti-tubulin (1:4,000; DSHB, 12g10). Secondary antibodies were alkaline phosphatase-conjugated

anti-rabbit and anti-mouse (both 1:5,000; Sigma-Aldrich, A3812, A3562), or fluorescent-conjugated IRDye 800CW anti-rabbit (1:13,000; LI-COR, 926–32211) and IRDye 800CW anti-mouse (1:13,000; LI-COR, 926–32210). The fluorescent membrane was scanned with an Odyssey CLx imager (LI-COR).

Bioinformatics

For species tree reconstruction, 302 eukaryotic BUSCO gene families were aligned with L-INS-I algorithm of MAFFT and trimming with trimAL (–strict) [37,38]. Phylogenetic reconstruction was performed with RAxML BlackBox in the CIPRES Science Gateway, using 1000 rapid bootstrap replicates and PROTGAMMAWAG model in the concatenated supermatrix, which was partitioned by genes [39]. Gene tree reconstruction was performed with the same pipeline and custom R scripts as before [40]. The gene tree was rooted and reconciled with the species tree using Notung 2.9 with 50% bootstrap support as the edge-weight threshold for topological rearrangements [41]. Duplication/loss events were mapped onto the species tree using Dollo parsimony with the compare pipeline [42,43]. CLUSTALW alignment of selected Atg8 homologs was carried out using Unipro UGENE v1.31.1 [43].

Statistical analysis

Quantification were always done using the original, unprocessed images. All experiments have been performed at least 3 times using independent biological samples. Fluorescent dots and the size of the gastric ceca were quantified by ImageJ (NIH). The Gaussian or non-Gaussian distribution of the data was checked by Prism 8.0.1 (GraphPad) software. For statistical analysis, ANOVA or two-tailed, two-sample unpaired t-test were performed when datasets were Gaussian for analyzing more than 3 or exactly 2 samples, respectively, and the Kruskal-Wallis test was used for analyzing multiple samples when one or more datasets were non-Gaussian. Error bars show standard error. Graphs and statistical tests were executed by Prism 8.0.1 (GraphPad) software.

Disclosure of potential conflict of interest

The authors declare that no conflicts of interest exist.

Funding

This work was supported by the Magyar Tudományos Akadémia [Momentum LP2014/2]; Nemzeti Kutatási Fejlesztési és Innovációs Hivatal [K132155]; Nemzeti Kutatási Fejlesztési és Innovációs Hivatal [GINOP-2.3.2-15-2016-00035]; Nemzeti Kutatási Fejlesztési és Innovációs Hivatal [GINOP-2.3.2-15-2016-00032]; Nemzeti Kutatási Fejlesztési és Innovációs Hivatal [KKP129797].

Acknowledgments

We thank Sarolta Pálfi and Szilvia Bozsó for their excellent technical assistance and Tamás Maruzs and Áron Szabó for their help with methods.

Funding

This work was supported by the Magyar Tudományos Akadémia [Momentum LP2014/2]; Nemzeti Kutatási Fejlesztési és Innovációs Hivatal [K132155]; Nemzeti Kutatási Fejlesztési és Innovációs Hivatal [GINOP-2.3.2-15-2016-00035]; Nemzeti Kutatási Fejlesztési és Innovációs Hivatal [GINOP-2.3.2-15-2016-00032]; Nemzeti Kutatási Fejlesztési és Innovációs Hivatal [KKP129797].

ORCID

András Jipa  <http://orcid.org/0000-0003-4880-7666>
 Viktor Vedelek  <http://orcid.org/0000-0002-0420-8226>
 Rita Sinka  <http://orcid.org/0000-0003-4040-4184>
 Gábor Juhász  <http://orcid.org/0000-0001-8548-8874>

References

- [1] Morishita H, Mizushima N. Diverse Cellular Roles of Autophagy. *Annu Rev Cell Dev Biol.* 2019;35(1):453–475.
- [2] Mizushima N. The ATG conjugation systems in autophagy. *Curr Opin Cell Biol.* 2019;63:1–10.
- [3] Nagy P, Á V, Kovács AL, et al. How and why to study autophagy in *Drosophila*: it's more than just a garbage chute. *Methods.* 2015;75:151–161.
- [4] Chang TK, Shrivage BV, Hayes SD, et al. Uba1 functions in Atg7- and Atg3-independent autophagy. *Nat Cell Biol.* 2013;15(9):1067–1078.
- [5] Xu T, Nicolson S, Denton D, et al. Distinct requirements of Autophagy-related genes in programmed cell death. *Cell Death Differ.* 2015;22(11):1792–1802.
- [6] Leader DP, Krause SA, Pandit A, et al. FlyAtlas 2: a new version of the *Drosophila melanogaster* expression atlas with RNA-Seq, miRNA-Seq and sex-specific data. *Nucleic Acids Res.* 2018;46(D1):D809–d15.
- [7] Vedelek V, Bodai L, Grezal G, et al. Analysis of *Drosophila melanogaster* testis transcriptome. *BMC Genomics.* 2018;19(1):697.
- [8] Betran E, Thornton K, Long M. Retroposed new genes out of the X in *Drosophila*. *Genome Res.* 2002;12(12):1854–1859.
- [9] Scott RC, Juhasz G, Neufeld TP. Direct induction of autophagy by atg1 inhibits cell growth and induces apoptotic cell death. *Curr Biol.* 2007;17(1):1–11.
- [10] Matthews BB, Dos Santos G, Crosby MA, et al. Gene Model Annotations for *Drosophila melanogaster*: impact of High-Throughput Data. G3 (Bethesda). 2015;5(8):1721–1736. .
- [11] Diao F, Ironfield H, Luan H, et al. Plug-and-play genetic access to *drosophila* cell types using exchangeable exon cassettes. *Cell Rep.* 2015;10(8):1410–1421.
- [12] Nezis IP, Simonsen A, Sagona AP, et al. Ref(2)P, the *Drosophila melanogaster* homologue of mammalian p62, is required for the formation of protein aggregates in adult brain. *J Cell Biol.* 2008;180(6):1065–1071.
- [13] Hegedus K, Takats S, Boda A, et al. The Ccz1-Mon1-Rab7 module and Rab5 control distinct steps of autophagy. *Mol Biol Cell.* 2016;27(20):3132–3142.
- [14] Kim M, Semple I, Kim B, et al. *Drosophila* Gyf/GRB10 interacting GYF protein is an autophagy regulator that controls neuron and muscle homeostasis. *Autophagy.* 2015;11(8):1358–1372.
- [15] Bhukel A, Beuschel CB, Maglione M, et al. Autophagy within the mushroom body protects from synapse aging in a non-cell autonomous manner. *Nat Commun.* 2019;10(1):1318.
- [16] Mauvezin C, Ayala C, Braden CR, et al. Assays to monitor autophagy in *Drosophila*. *Methods.* 2014;68(1):134–139.
- [17] Senos DR, BS U, DL J. EGFR Signaling Stimulates Autophagy to Regulate Stem Cell Maintenance and Lipid Homeostasis in the *Drosophila* Testis. *Cell Rep.* 2020;30:1101–16.e5.

- [18] Kiss V, Jipa A, Varga K, et al. *Drosophila* Atg9 regulates the actin cytoskeleton via interactions with profilin and Ena. *Cell Death Differ.* 2020;27(5):1677–1692.
- [19] Fabian L, Brill JA. *Drosophila* spermiogenesis: big things come from little packages. *Spermatogenesis.* 2012;2(3):197–212.
- [20] Zhu Y, Yin Q, Wei D, et al. Autophagy in male reproduction. *Syst Biol Reprod Med.* 2019;65:265–272.
- [21] Al-Younes HM, Al-Zeer MA, Khalil H, et al. Autophagy-independent function of MAP-LC3 during intracellular propagation of *Chlamydia trachomatis*. *Autophagy.* 2011;7(8):814–828.
- [22] Cali T, Galli C, Olivari S, et al. Segregation and rapid turnover of EDEM1 by an autophagy-like mechanism modulates standard ERAD and folding activities. *Biochem Biophys Res Commun.* 2008;371(3):405–410.
- [23] Reggiori F, Monastyrska I, Verheije MH, et al. Coronaviruses Hijack the LC3-I-positive EDEMosomes, ER-derived vesicles exporting short-lived ERAD regulators, for replication. *Cell Host Microbe.* 2010;7(6):500–508.
- [24] Juhasz G, Erdi B, Sass M, et al. Atg7-dependent autophagy promotes neuronal health, stress tolerance, and longevity but is dispensable for metamorphosis in *Drosophila*. *Genes Dev.* 2007;21(23):3061–3066.
- [25] Guo T, Nan Z, Miao C, et al. The autophagy-related gene Atg101 in *Drosophila* regulates both neuron and midgut homeostasis. *J Biol Chem.* 2019;294:5666–5676.
- [26] Kim M, Sandford E, Gatica D, et al. Mutation in ATG5 reduces autophagy and leads to ataxia with developmental delay. *Elife.* 2016; 5:e12245
- [27] Varga K, Nagy P, Arsikin Csordas K, et al. Loss of Atg16 delays the alcohol-induced sedation response via regulation of Corazonin neuropeptide production in *Drosophila*. *Sci Rep.* 2016;6(1):34641.
- [28] Santel A, Blumer N, Kampfer M, et al. Flagellar mitochondrial association of the male-specific Don Juan protein in *Drosophila* spermatozoa. *J Cell Sci.* 1998;111(Pt 22):3299–3309.
- [29] Siddall NA, Hime GRA. *Drosophila* toolkit for defining gene function in spermatogenesis. *Reproduction.* 2017;153(4):R121–r32.
- [30] Port F, Chen HM, Lee T, et al. Optimized CRISPR/Cas tools for efficient germline and somatic genome engineering in *Drosophila*. *Proc Natl Acad Sci U S A.* 2014;111(29):E2967–76.
- [31] Kondo S, Ueda R. Highly improved gene targeting by germline-specific CAS9 expression in *Drosophila*. *Genetics.* 2013;195(3):715–721.
- [32] Takáts S, Nagy P, Varga Á, et al. Autophagosomal Syntaxin17-dependent lysosomal degradation maintains neuronal function in *Drosophila*. *J Cell Biol.* 2013;201(4):531–539.
- [33] Takáts S, Piracs K, Nagy P, et al. Interaction of the HOPS complex with Syntaxin 17 mediates autophagosome clearance in *Drosophila*. *Mol Biol Cell.* 2014;25(8):1338–1354.
- [34] Piracs K, Nagy P, Varga A, et al. Advantages and limitations of different p62-based assays for estimating autophagic activity in *Drosophila*. *PLoS One.* 2012;7(8):e44214.
- [35] Laurinyecz B, Vedelek V, Kovacs AL, et al. Sperm-Leucylaminopeptidases are required for male fertility as structural components of mitochondrial paracrystalline material in *Drosophila melanogaster* sperm. *PLoS Genet.* 2019;15(2): e1007987.
- [36] Takats S, Glatz G, Szenci G, et al. Non-canonical role of the SNARE protein Ykt6 in autophagosome-lysosome fusion. *PLoS Genet.* 2018;14(4):e1007359.
- [37] Seppy M, Manni M, Zdobnov EM. BUSCO: assessing genome assembly and annotation completeness. *Methods Mol Biol.* 2019;1962:227–245.
- [38] Katoh K, Standley DM. MAFFT multiple sequence alignment software version 7: improvements in performance and usability. *Mol Biol Evol.* 2013;30(4):772–780.
- [39] Stamatakis A. RAxML version 8: a tool for phylogenetic analysis and post-analysis of large phylogenies. *Bioinformatics.* 2014;30(9):1312–1313.
- [40] Merenyi Z, Prasanna AN, Wang Z, et al. Unmatched level of molecular convergence among deeply divergent complex multicellular fungi. *Mol Biol Evol.* 2020;37(8):2228–2240.
- [41] Darby CA, Stolzer M, Ropp PJ, et al. Xenolog classification. *Bioinformatics.* 2017;33:640–649.
- [42] Nagy LG, Ohm RA, Kovacs GM, et al. Latent homology and convergent regulatory evolution underlies the repeated emergence of yeasts. *Nat Commun.* 2014;5(1):4471.
- [43] Okonechnikov K, Golosova O, Fursov M. Unipro UGENE: a unified bioinformatics toolkit. *Bioinformatics.* 2012;28(8):1166–1167.